

Ligand-Centered Redox in Nickel(II) Complexes of 2-(Arylazo)pyridine and Isolation of 2-Pyridyl-Substituted Triaryl Hydrazines via Catalytic N-Arylation of Azo-Function

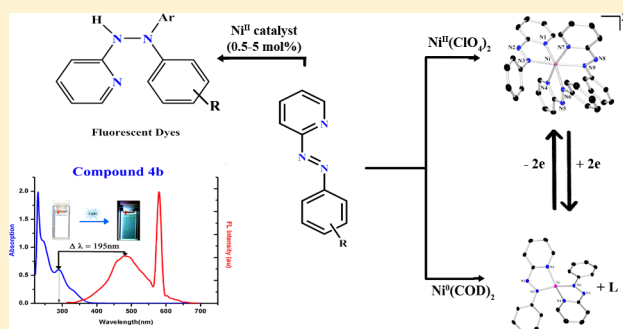
Debabrata Sengupta,[†] Pradip Ghosh,[†] Tanmay Chatterjee,[‡] Harashit Datta,[†] Nanda D. Paul,^{†,§} and Sreebrata Goswami^{*,†}

[†]Department of Inorganic Chemistry, Indian Association for the Cultivation of Science, Jadavpur, Kolkata 700 032, India

[‡]Department of Organic Chemistry, Indian Association for the Cultivation of Science, Jadavpur, Kolkata 700 032, India

Supporting Information

ABSTRACT: A series of nickel complexes of 2-(arylazo)pyridine have been synthesized, and the precise structure and stoichiometry of the complexes are controlled by the use of different metal precursors. Molecular and electronic structures of the isolated complexes are scrutinized thoroughly by various spectroscopic techniques, single crystal X-ray crystallography, and density functional theory (DFT). Two different classes of Ni(II) complexes are identified where the ligands bind as neutral or anion radicals in the respective metal complexes. These are shown to be chemically interconvertible, and their characterization confirmed that the redox series is entirely ligand-centered without affecting the bivalent oxidation state of the metal ion. An efficient method of Ni(II) catalyzed N-arylation of 2-(arylazo)pyridine substrates has been elaborated. The chemical reactions have led to isolation of strongly fluorescent 2-pyridyl-substituted hydrazone derivatives, which have been characterized thoroughly. Three-dimensional X-ray structure of a hydrazone molecule, 2-(2-(naphthalen-1-yl)-2-phenylhydrazinyl)pyridine, is reported. Isolated hydrazines satisfy all the prerequisites of an ideal dye with moderate absorptive property, large Stokes shift, high quantum yields, and high photostability.



INTRODUCTION

Over the years, studies of the electronic structures of the complexes have been the key point of exploration in the field of redox noninnocent ligand chemistry.^{1–8} However, during recent years the practiced philosophy has experienced a gradual shift toward the application domain, primarily to nonconventional ligand-based chemical reactions. For example, a number of practical applications of transition-metal–ligand radical complexes in catalytic and enzymatic processes have emerged,^{9–12} and the synergy between metal and ligand redox has been a subject of recent reviews.¹³

Out of our interest in coordination chemistry of redox noninnocent azo-aromatics, herein we have explored redox properties of a series of nickel complexes of 2-(arylazo)pyridines. Subsequent development of a potent Ni(II)-salt catalyzed N-arylation of 2-(arylazo)pyridines, indeed, adds an unique dimension to this domain. The key to the above phenomenon apparently is associated with facile reduction of coordinated azo-function of the ligand. To give a brief introduction of catalytic potential of the reference catalytic reaction, it must be appreciated that N-arylation reactions are noteworthy in the context of synthesis of tri/tetra-aryl hydrazines, which are high-valued chemical compounds known for their extensive use in pharmaceutical and agricultural

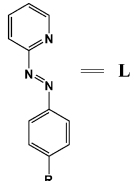
industries.^{14,15} Moreover, 2-pyridyl-substituted hydrazines are of special importance because of their efficiency to act as ligands that result in their potential applications in nuclear medicines.^{16–20} Notably these are usually synthesized by Pd-catalyzed N-arylation of diaryl hydrazines/hydrazones;²¹ however, only recently limited examples of Pd- or Au-complex catalyzed coupling between activated azo compounds and aryl boronic acids have been added to the literature.^{22–24} Herein we have reported high yield catalytic N-arylation of 2-(arylazo)pyridine using a base metal nickel(II) salt as catalyst, and the synthetic protocol leads to the isolation of a number of strongly fluorescent triarylhydrazine dyes, which are unavailable in literature.

In the upcoming sections we deal with synthesis and full characterizations of the Ni-complexes along with their redox-induced interconversions. Moreover, our journey to the development of Ni(II)-catalyzed N-arylation of azo-function in 2-(arylazo)pyridine substrate has also been taken up in detail.

Received: July 11, 2014

Published: November 5, 2014

Chart 1

	R	L	Complex					
	H	L ^a	[1a] ²⁺	[Ni ^{II} (L ^a) ₃] ²⁺	2a	Ni ^{II} (L ^a) ₂ Cl ₂	3a	Ni ^{II} (L ^{a•-}) ₂
Cl	L ^b	[1b] ²⁺	[Ni ^{II} (L ^b) ₃] ²⁺	2b	Ni ^{II} (L ^b) ₂ Cl ₂	3b	Ni ^{II} (L ^{b•-}) ₂	

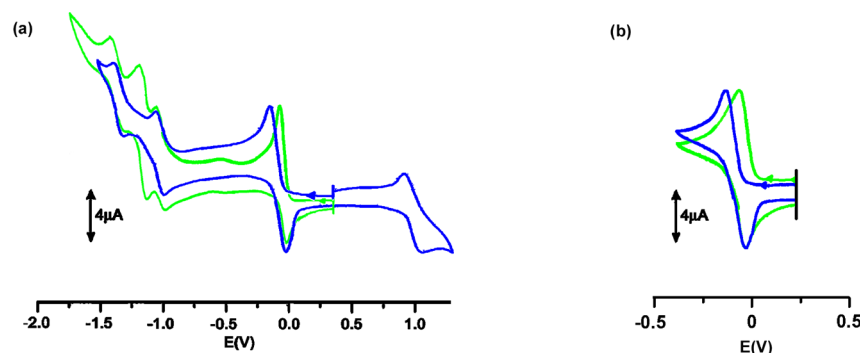


Figure 1. Cyclic voltammograms of the complexes, [1a](ClO₄)₂ (green) and 2a (blue), in dichloromethane in different voltage windows: (a) +1.2 V to -1.75 V and (b) +0.25 V to -0.50 V.

Table 1. Cyclic Voltammetric Data^{a,b} of the Complexes [1](ClO₄)₂ and 2

compd	oxidation $E_{1/2}$ ^c V (ΔE_p , mV)	reduction $E_{1/2}$ ^c V (ΔE_p , mV)
[1a](ClO ₄) ₂		-0.05(43), -1.03(70), -1.18(110), -1.43(90)
[1b](ClO ₄) ₂		-0.04(40), -1.01(75), -1.15(105), -1.41(90)
2a	1.01(130) ^d	-0.15(48), -1.00(80), -1.39(90)
2b	1.05(125) ^d	-0.12(47), -0.95(85), -1.36(95)

^aIn a dichloromethane solution, supporting electrolyte Bu₄NClO₄ (0.1 M), and reference electrode Ag/AgCl. ^bSolute concentration ca. 10⁻³ M. ^c $E_{1/2} = 0.5(E_{pa} + E_{pc})$, where E_{pa} and E_{pc} are anodic and cathodic peak potentials, respectively; $\Delta E_p = E_{pa} - E_{pc}$; scan rate = 50 mV s⁻¹. ^dQuasireversible.

RESULTS AND DISCUSSION

Chemical Reactions. The work began with an investigation of redox properties of previously reported²⁵ Ni²⁺ complexes of 2-(arylazo)pyridine ligands (L^{a,b}): [Ni^{II}(L^{a,b})₃](ClO₄)₂ and Ni^{II}(L^{a,b})₂Cl₂ (see Chart 1 for complex and ligand numbering scheme).

Cyclic voltammetric experiments of the two Ni complexes, [1a]²⁺ and 2a, were carried out in dichloromethane using tetrabutylammonium perchlorate (TBAP) as the supporting electrolyte, and the reported potentials are all referenced to the Ag/AgCl electrode. The complexes, under study, displayed multiple waves as shown in Figure 1a,b. The cationic complex [1a]²⁺ showed four reversible/quasireversible waves in the range ±1.5 V at -0.05, -1.03, -1.18, and -1.43 V. Out of these four reductive waves, i_p for the first redox couple (at -0.05 V) is significantly (~2.7 times) higher than that of the other three single-electron waves. Furthermore, peak-to-peak separation (ΔE_p) for the couple is in the range 40–43 mV (<59 mV), and the complex in principle can accept^{4d} maximum of six electrons. Exhaustive electrolysis at -0.5 V resulted in chemical conversion, [1a]²⁺ → 3a + L^a (vide supra). The dichloro complex 2a also exhibited three reversible reductive waves at -0.15, -1.00, and -1.39 V, and another oxidative quasireversible wave at +1.01 V was also observed. In this latter complex, the reductive wave appearing at the least cathodic potential is also characterized as a single step two-electron transfer process

but is shifted cathodic by 0.1 V than that of the corresponding tris-chelate. Their cyclic voltammograms are shown in Figure 1, and the data are collected in Table 1.

The above results indicate that Ni^{II}-L complexes undergo single step two-electron reductions as it happens²⁶ in the complex, [Ni(bpy)₃]²⁺ (bpy = 2,2'-bipyridine). Exhaustive electrolysis of [1a]²⁺ and 2a at -0.5 V led to a similar color change of the test solutions. Their initial green colors became brown on electrolysis. The brown solutions, generated as above, are hyperactive and undergo fast chemical decomposition to give a mixture of unidentified products.

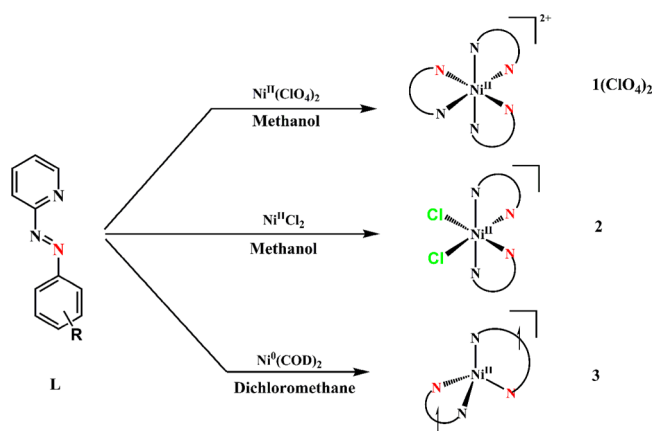
The two aforesaid compounds [1a]²⁺ and 2a were then subjected to chemical reductions in methanol using Zn metal (powder) as reducing agent in inert conditions (in a glovebox). In each case a brown solution resulted, and subsequent workup (see Experimental Section) of the solution formed single crystals, which were suitable for X-ray diffraction studies. Characterization (see latter) of the products, obtained from the above two reactions, indicated that these two are identical in all respects with chemical composition: [Ni^{II}(L^{a•-})₂], 3a (L^{a•-} = one electron reduced azo anion radical). It may be worthwhile here to compare this observation with the redox-induced chemical transformation of [Ni(bpy)₃]²⁺. It has been shown²⁶ before that the latter complex undergoes single step two-electron reduction to [Ni⁰(bpy)₃], and is followed by a fast loss of one bpy ligand to give an unstable tetracoordinated complex [Ni⁰(bpy)₂]. In the present case, however, there is an additional

internal electron transfer process in $[\text{Ni}^0(\text{L}^{\bullet})_2]$, one-electron transfer from $\text{Ni}(0)$ to each of the two coordinated ligands, which produced the complex **3a**. This is as expected since **L** undergoes reduction more easily²⁷ than **bpy**. On the basis of the above results, a chemical reaction between a labile Ni^0 precursor, $[\text{Ni}^0(\text{COD})_2]$ (COD = cyclooctadiene), and L^{\bullet} in 1:2 molar proportion was planned, which proceeded as anticipated with the formation of the same diradical complex, **3a** in a high yield (90%). This result is parallel to our recent knowledge^{4b-f} on the chemical reactivities of **L** with electron-rich metal precursors. The geometry of the complex **3a** is distorted tetrahedral, and it is diamagnetic ($S = 0$). Thorough analyses of its electronic structure (see below) have revealed that it is a $\text{Ni}(\text{II})$ complex with a high-spin d^8 electron configuration ($S_{\text{Ni}} = 1$) where the two spins on Ni^{II} are coupled intramolecularly and antiferromagnetically to two coordinated ligand π^* radicals $\text{L}^{\bullet-}$ ($S_{\text{L}} = 1/2$).

Another set of similar experiments using a *p*-chloro-substituted ligand, L^{b} , also showed similar redox behavior for $[\mathbf{1b}]^{2+}$ and **2b** and produced $[\text{Ni}^{\text{II}}(\text{L}^{\text{b}\bullet-})_2]$, **3b**, in high yields.

Interestingly, the aforementioned complexes are found to be chemically interconvertible using appropriate reagents. For example, the hexacoordinated complex $[\mathbf{1}]^{2+}$ undergoes facile reduction to **3** by Zn metal in an inert atmosphere; complex **3**, on the other hand, can be reverted to $[\mathbf{1}]^{2+}$ by oxidation with 2 mol equiv of ferrocenium hexafluorophosphate in the presence of 1 mol equiv of **L**. Similar oxidations of **3** with X_2 ($\text{X} = \text{Cl}, \text{I}$), in turn, produced the complexes $\text{Ni}^{\text{II}}\text{L}_2\text{X}_2$, **2**, in high yields. Chemical synthesis of the complexes and their interconversions are shown in Schemes 1 and 2, respectively.

Scheme 1. Reaction of 2-(Arylazo)pyridine Ligand with Three Metal Precursors



Characterization: X-ray Crystallography and Spectroscopy.

As noted above, syntheses of the complexes $[\mathbf{1}](\text{ClO}_4)_2$ and **2** were known, but their X-ray structures and redox properties were not available.²⁵ In order to make comparative studies, their complete characterizations are made along with that of **3**. All the complexes of L^{\bullet} uniformly formed excellent crystals which were used for their X-ray structure determination. Crystallographic details of the three compounds, $[\mathbf{1a}](\text{ClO}_4)_2$, **2a**, and **3a**, are collected in Table 2, key bond lengths and angles of these complexes are in Table 3, and ORTEP images of all the complexes are in Figure 2. Crystallographic details and the ORTEP of $\text{Ni}(\text{L}^{\bullet})_2\text{I}_2$ are submitted as Supporting Information (Figure S2 and Table S1).

Figure 2 shows that the two complexes $[\mathbf{1a}]^{2+}$ and **2a** have approximate octahedral coordination about the nickel center, but complex **3a** adopts a distorted tetrahedral arrangement. Complex $[\mathbf{1a}]^{2+}$ is isolated as a *mer*-isomer. Interestingly, the unit cell of the latter complex, **3a**, contains two geometrical isomeric tetrahedral units (see Supporting Information, Scheme S1). Such a possibility exists in distorted tetrahedral complexes²⁸ though their bond parameters remain more or less similar. The two isomers A and B both possess C_2 symmetry, but the interatomic distances between the coordinated nitrogen are different: for example, $\text{N}(\text{py}1) - \text{N}(\text{py}2)$, 3.111 Å (isomer A) and 3.551 Å (isomer B). The bond parameters of the isomers are tabulated in Supporting Information (Table S3). Isomer A is energetically slightly higher than isomer B by 0.69 kcal/mol. It is likely that two isomers A and B easily interconvert in solution which resulted in a simplified ¹H NMR spectrum of complexes **3a,b**. The N–N bond lengths in complexes $[\mathbf{1a}](\text{ClO}_4)_2$ and **2a** lie in a narrow window between 1.24 and 1.27 Å which is characteristic of neutral ligands, but these two lengths are considerably elongated in **3a**: 1.337(4) and 1.325(5) Å, respectively. Bond length elongation in **3a** is an indication⁴ that the ligands are reduced in this complex. Significant changes of Ni– N_{azo} lengths in moving from $[\mathbf{1a}]^{2+}/\mathbf{2a}$ to **3a** are also indicative of changes in the electronic structure in $[\mathbf{1a}]^{2+}/\mathbf{2a}$ versus **3a**: while the Ni– N_{azo} ($[\mathbf{1a}]^{2+}$ and **2a**) is longer than Ni– N_{py} counterparts (av 2.17 Å vs 2.06 Å), the opposite is true in **3a** (1.86 Å vs 1.92 Å). These changes of bond lengths indicate a transition on neutral ligand in $[\mathbf{1a}]^{2+}$ and **2a**, where the azo group is a weak donor²⁹ than N_{py} to an azo-anion ligand in **3a**. As a whole, the structural and physical properties are consistent with accumulation of negative charge^{4d} on the azo groups in **3a**. Final picture of assignment of oxidation state of the complex **3a** will be discussed in the section dealing with electronic structure calculations.

Scheme 2. Redox-Driven Interconversion of Nickel Complexes

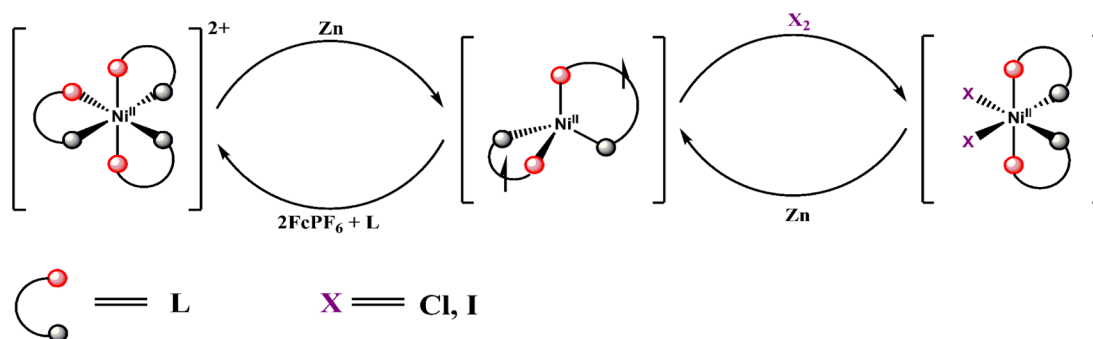


Table 2. Crystallographic Details of Complexes [1a](ClO₄)₂, 2a, 3a, and 4b

	[1a](ClO ₄) ₂	2a	3a	4b
empirical formula	C ₃₃ H ₂₇ N ₉ Cl ₂ O ₈ Ni	C ₂₃ H ₂₀ N ₆ Cl ₄ Ni	C ₂₂ H ₁₈ N ₆ Ni	C ₂₁ H ₁₇ N ₃
molecular mass	807.23	580.94	425.11	311.38
<i>T</i> (K)	293	293	150	293
cryst syst	monoclinic	monoclinic	orthorhombic	monoclinic
space group	<i>P</i> 2 ₁ / <i>c</i>	<i>P</i> 2 ₁ / <i>c</i>	<i>Pna</i> 2 ₁	<i>P</i> 2 ₁ / <i>c</i>
<i>a</i> (Å)	9.3581(7)	9.276(5)	32.4726(16)	14.066(6)
<i>b</i> (Å)	9.6869(7)	17.451(5)	8.6450(4)	7.975(4)
<i>c</i> (Å)	39.014(3)	15.923(5)	13.5478(7)	14.885(7)
α (deg)	90	90	90	90
β (deg)	93.296(2)	91.812(5)	90	99.335(14)
γ (deg)	90	90	90	90
<i>V</i> (Å ³)	3530.9(5)	2577.3(18)	3803.2(3)	1647.4(13)
<i>Z</i>	4	4	8	4
<i>D</i> _{calcd} (g/cm ³)	1.519	1.497	1.485	1.255
cryst dimens (mm ³)	0.12 × 0.15 × 0.19	0.14 × 0.18 × 0.20	0.09 × 0.16 × 0.18	0.08 × 0.10 × 0.12
θ range for data collection (deg)	1.0–32.1	1.7–25.7	1.3–27.5	1.47–24.89
GOF	1.04	1.01	1.06	1.025
reflns collected	53 081	32 145	50 725	18 737
unique reflns	12 353	4895	8393	2846
final <i>R</i> indices [<i>I</i> > 2 σ (<i>I</i>)]	<i>R</i> = 0.0431 w <i>R</i> 2 = 0.1074	<i>R</i> = 0.0374 w <i>R</i> 2 = 0.1037	<i>R</i> = 0.0357 w <i>R</i> 2 = 0.0905	<i>R</i> = 0.0520 w <i>R</i> 2 = 0.1579

Table 3. Selected Bond Distances and Bond Angles of Complexes [1a](ClO₄)₂, 2a, and 3a

param	experimental			calcd 3a isomer A
	[1a](ClO ₄) ₂	2a (X = Cl)	3a isomer A	
Ni1–N1	2.0630(16)	2.063(3)	1.918(3)	1.922
Ni1–N3	2.1681(14)	2.158(3)	1.864(3)	1.866
Ni1–N4	2.0406(15)	2.072(3)	1.925(3)	1.926
Ni1–N6	2.0919(15)	2.143(3)	1.870(3)	1.883
Ni1–N7	2.0525(15)			
Ni1–N9	2.1224(14)			
N2–N3	1.259(2)	1.258 (3)	1.337(4)	1.334
N5–N6	1.255(2)	1.256(3)	1.325(5)	1.331
N8–N9	1.262(2)			
Ni1–Cl1		2.3607(15)		
Ni1–Cl2		2.3723(16)		
N1–Ni1–N3	75.13(6)	74.46(10)	80.81(14)	80.11
N4–Ni1–N6	76.21(6)	75.02(9)	80.59(13)	80.85
N7–Ni1–N9	76.10(5)			
Cl1–Ni1–Cl2		97.48(3)		
dihedral angle ^a			59.52	62.61

^aAngle between the two planes: 1 (defined by Ni1–N1–C5–N2–N3) and 2 (defined by Ni1–N4–C16–N5–N6).

The compound [1](ClO₄)₂ behaves as a 1:2 electrolyte in acetonitrile solvent, while the solutions of 2 and 3 are nonelectrolytic. Magnetic susceptibility measurements at 300 K for complexes [1a](ClO₄)₂ and 2a indicate that these are paramagnetic with magnetic moments, 2.42 and 2.43 μ_B , respectively, which are close to the spin-only value for mononuclear Ni^{II} (*S* = 1) ion. The tetrahedral complexes, [3a,b], on the other hand, are diamagnetic (*S* = 0) and displayed highly resolved ¹H NMR spectra. A representative spectrum of 3a in CDCl₃ is displayed in Figure 3, and that of 3b is submitted as Supporting Information (Figure S4). In Figure 3, all seven aromatic proton resonances for one ligand are

visible in the range δ 7.0–10.5. ¹³C NMR data of these are collected in the Experimental Section, and the spectra of 3a and 3b are deposited as Supporting Information Figures S3 and S4(b). Complexes [3a,b] are intensely brown and absorb strongly in the 200–450 nm range which are associated with weak and broad transition in the near IR region (λ_{\max} = 780 nm). The electronic spectra of the reported complexes, [1a,b]²⁺ and [2a,b], correspond²⁵ well with the published data. Their UV–vis spectral data are collected in the Experimental Section.

Electronic Structure Analysis. To have an insight into the electronic structure of complex 3a we have performed series of calculations using DFT at the B3LYP level which is implemented at G09W program package. Two models were primarily considered for the diamagnetism (*S* = 0) for the Ni(L)₂ complex, 3a: (i) high-spin Ni^{II} (*S*_{Ni} = 1) coupled antiferromagnetically to two ligand radicals (*S*_L = *S*_L = +1/2) or (ii) Ni^I (*S*_{Ni} = 1/2) coupled antiferromagnetically to a single unpaired electron, either localized on a single ligand or delocalized over both. The most preferred ground-state electronic structure of the complex 3a was found to be a high-spin Ni(II) ion antiferromagnetically coupled to two azo-anion radicals (L^{•−}). The calculated bond distances derived from the BS(2,2) calculation also matched well with the experimental bond parameters. The selected bond distances and bond angles are collected in Table 3. Notably, the BS(2,2) calculated dihedral angle between the two metallacycles (plane 1 defined by Ni1–N1–C5–N2–N3 and plane 2 defined by Ni1–N4–C16–N5–N6) in 3a is 62.61° which is in excellent agreement with the experimental value of 59.52°. The qualitative MO diagram (Figure 4) reveals two metal-based singly occupied molecular orbitals (SOMOs) (*d*_{xy} and *d*_{xz}) in the spin-up manifold which are coupled to two SOMOs, which are primarily the lowest unoccupied molecular π^* orbitals of the neutral ligand, in the spin-down manifold with overlaps of 0.56 and 0.69, respectively. This indicates the existence of strong antiferromagnetic interactions between two unpaired electrons of metal and two ligand radicals. However, in a tetrahedral geometry, the π^* orbitals would interact with *d*

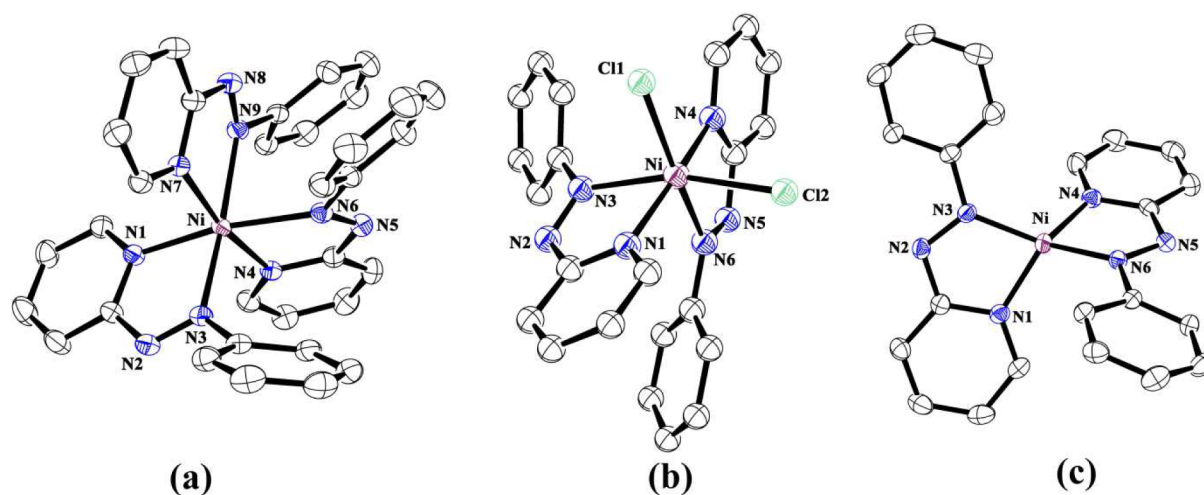


Figure 2. ORTEP representation of the complexes: (a) $[1a]^{2+}$, (b) **2a**, and (c) **3a** (isomer A) at 50% probability ellipsoid. The counteranions, for $[1a]^{2+}$, and hydrogen atoms of all molecules are omitted for clarity.

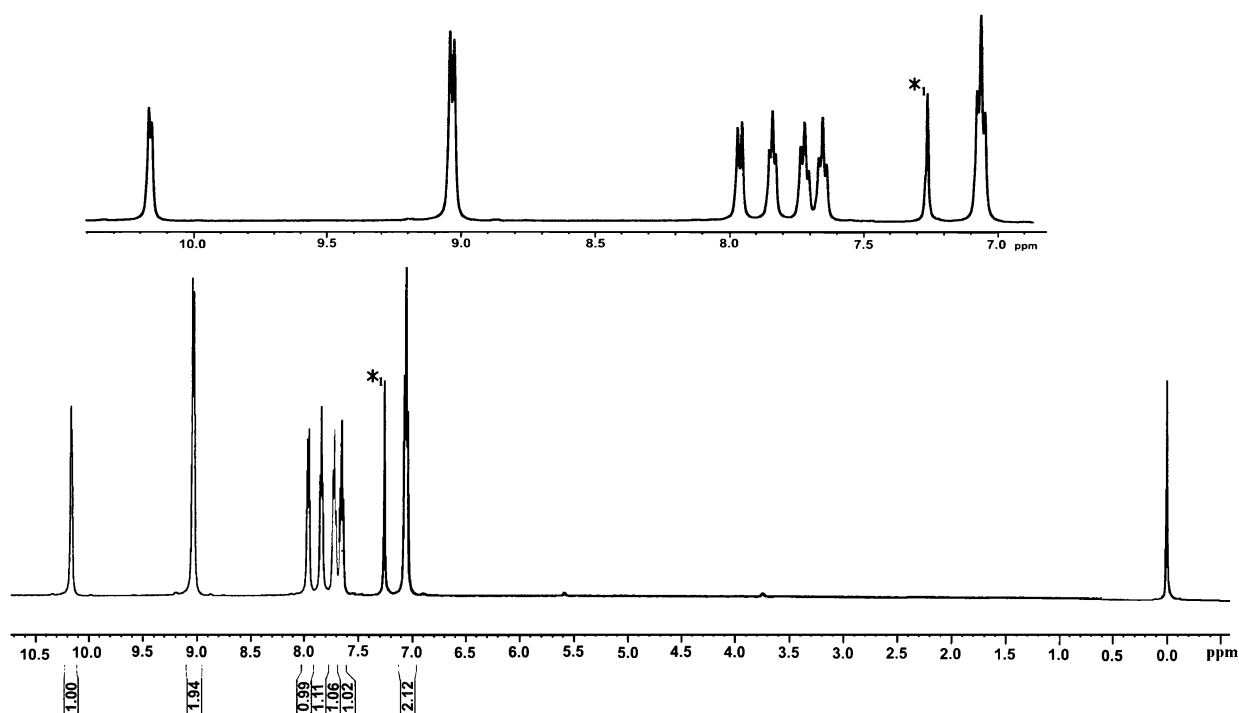


Figure 3. ^1H NMR spectrum of the complex **3a** in CDCl_3 solution (*₁, solvent) (inset shows aromatic proton resonances).

orbitals that are orthogonal, and long-range ligand–ligand coupling of two nearly orthogonal ligand orbitals is impossible; hence, we have discarded²⁸ the possibility of Ni^{II} ($S_{\text{Ni}} = 0$) with two antiferromagnetically coupled ligand radicals ($S_L = \pm 1/2$).

Another possibility of $[\text{Ni}^0(\text{L}^a)_2]$ was also considered for which a restricted calculation was employed. Energy of the optimized structure is higher than that of the broken symmetry calculation, BS(2,2), by 4.6 kcal/mol. Moreover, metrical parameters for the latter description are closer to the observed structure (see Supporting Information Table S4).

Furthermore, the spin-density plot (Figure 5) derived from broken-symmetry calculation reinforces singlet ground state due to opposing Mulliken spin populations on Ni (1.40) and ligands (-0.70 per L). Moreover, the presence of a net spin density >1.0 and two approximately singly occupied d orbitals is consistent with the high-spin Ni^{II} ($S_{\text{Ni}} = 1$) description. The

ligands are therefore effectively reduced by one electron ($S_L = S_L = 1/2$) each, driving the significant elongation of two $d_{\text{N-N}}$ distances relative to those in $[1a]^{2+}$ and **2a** (1.33 vs 1.25 Å). Interestingly, some spin density is delocalized over the *ortho* and *para* carbon atom of the phenyl ring, the effect of which is manifested in the deshielding³⁰ of aromatic proton resonances in the ^1H spectra of the complexes **[3a,b]**.

Chemical Catalysis. From the above results it may be concluded that $\text{Ni}^{\text{II}}\text{-L}$ complexes are susceptible to single step two-electron reduction processes with synergistic metal–ligand participation and are associated with reversible chemical transfer of ligand(s) dissociation/association in solution. In the present context it is worth noting that it has now been history that transition-metal complexes of noble metals like Pd, Rh, Pt, etc. dominate the catalytic bond fusion reactions because of their ability to participate in two-electron transfer

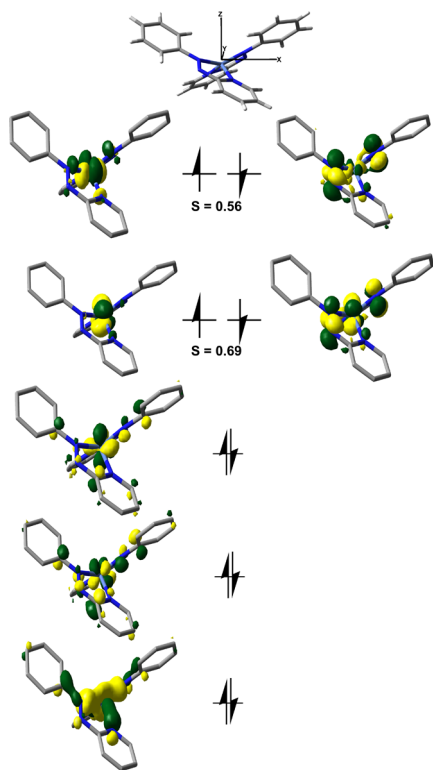


Figure 4. Qualitative MO diagram of the magnetic orbitals derived from BS(2,2) calculation of $[\text{Ni}(\text{L}^{a*})_2]$. The spatial overlap (S) of the corresponding α and β orbitals is given.

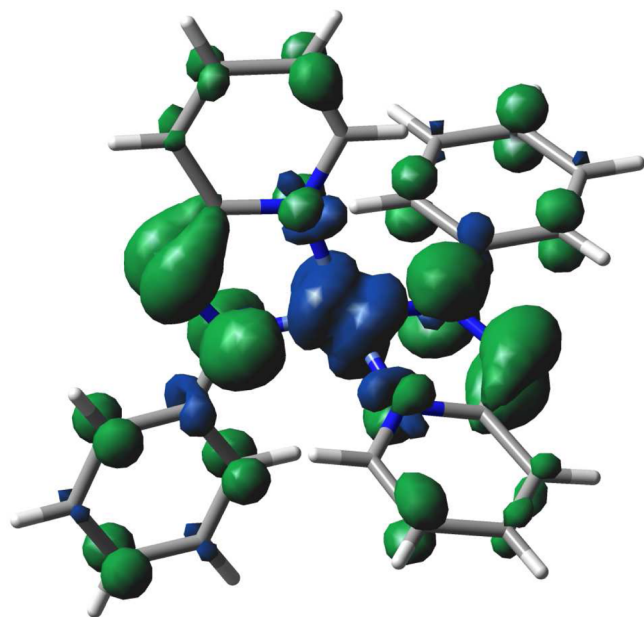


Figure 5. Spin density plot of the complex, $[\text{Ni}(\text{L}^{a*})_2]$, **3a**, derived from BS(2,2) calculation.

processes (oxidative addition and reductive elimination) which in fact are the elementary steps in C–C and C–heteroatom bond making reactions.^{31,32} Electron storage ability of the reference azoareomatics, as demonstrated herein, has opened up the scope of using these and similar 3d metal complexes in catalytic coupling reactions.

Accordingly a stoichiometric chemical reaction, as shown in Scheme 3, we tried to look for the corresponding C–C coupled

product (Suzuki coupling). However, the reaction did not proceed as expected, but it produced 2-pyridyl-substituted triaryl hydrazine as the only product, and aryl halide remained unreacted.

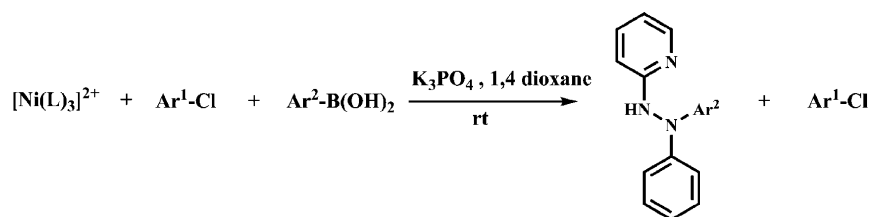
Consequently, an investigation of nickel-catalyzed arylation of azo-function with aryl boronic acid was initiated. Finally, we were successful in developing a Ni^{II} salt ($\text{Ni}(\text{ClO}_4)_2$ or NiCl_2) catalyzed N-arylation of 2-(aryloxy)pyridines under mild conditions as shown in Scheme 4. Isolated products and their yields are collected in Table 4.

Table 4 provides information on the impact of catalyst and temperature on the efficiency of this process. In absence of catalyst no reaction occurs even at 450 K. The transformation exhibits a broad scope and a high tolerance for a variety of functional groups, as shown in Table 5. The reaction is applicable to a wide range of substituted aryl, heteroaryl, or polycyclic groups. Typical polycyclic groups used are naphthyl, anthracenyl, pyrynyl, fluorinyl, etc. Furthermore, both electron-rich and electron-poor arylboronic acids participated in the reactions with ease. It may also be noted that the aryl–halogen bond remained intact during the catalysis, which demonstrates that a potential Buchwald–Hartwig or Suzuki cross-coupling reaction cannot compete under the present conditions of catalysis. We are particularly interested in the molecules that contain fluorophoric groups like naphthalene, anthracene, pyrene, fluorine, etc. to expand their application possibilities further.^{14,33}

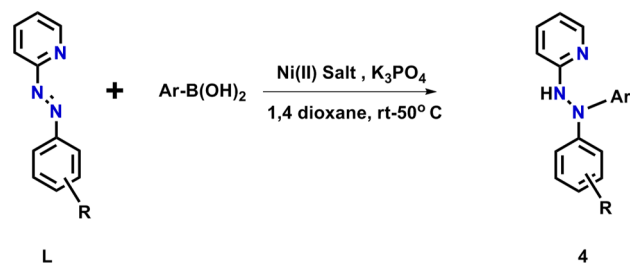
Characterization of Hydrazines: Spectroscopic and X-ray Structure. All triaryl hydrazines, isolated as above, were fully characterized by ^1H NMR, ^{13}C NMR, ESI-MS, and IR spectroscopy. The N–H and N–N stretching frequencies for these appeared³⁴ at around 3435 and 1145 cm^{-1} , respectively, in the IR spectra of the compounds. These compounds displayed multiple signals in the aromatic region. However, the N–H proton was not detectable in CDCl_3 solution. This might be attributed³⁵ by reversible dimerization of the 2-amino-pyridine group in CDCl_3 solution. This will lead to broadening of the N–H resonance to that extent that it is difficult to detect in CDCl_3 solution. However, this dimerization is inhibited in d_6 -DMSO solvent, because of its strong hydrogen bond acceptor nature. Accordingly, the ^1H NMR spectrum of compound **4b** (in d_6 -DMSO) displayed a characteristic N–H proton signal at 9.48 ppm, which disappeared on D_2O shake. Selected spectral data of the compound are collected in the Experimental Section, and complete details of spectral characterizations of the compounds are submitted as Supporting Information.

Three-dimensional X-ray structure determination of a representative compound, **4b**, is used to further authenticate the identity of this class of triarylhydrazines. Suitable crystals were obtained by slow evaporation of the solution of **4b** in a mixed solvent, dichloromethane–hexane (1:1) mixture. An ORTEP of it is shown in Figure 6. Examination of N–N bond distance, $d_{\text{N2-N3}}$, 1.401(5) Å, clearly reveals that it is a single bond, as expected for a hydrazine molecule. Moreover, the three bond angles around N3 are N2–N3–C12 114.36(19)°, C6–N3–C12 119.01(17)°, and C6–N3–N2 112.54(17)°, respectively, and that around N2 also lies in the similar range signifying that these two N atoms are sp^3 -hybridized. Selected bond parameters are collected in Table 6, and crystallographic details are presented in Table 2. As far we are aware, three-dimensional X-ray structure of this class of compound is unavailable in literature.

Scheme 3. Attempted C–C Coupling

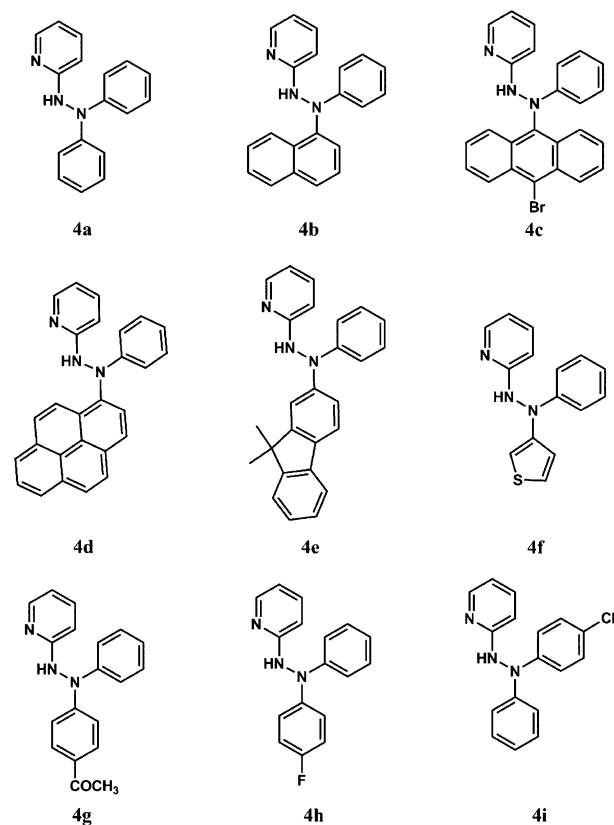


Scheme 4. Ni(II)-Catalyzed Coupling of 2-(Arylazo)pyridine with Aryl Boronic Acid



On the Arylation Reaction. Our present knowledge on the above N-arylation reaction is not sufficient to assess the mechanism as yet. However, a few observations related to the reactions are noted below. It is envisaged from the following observations that modified redox properties of the coordinated 2-(arylazo)pyridines play the controlling role in this transformation. First, formation of a coordinated nickel complex during the course of the reaction was established by trapping a green product that was observed to form in the reaction mixture by the use of higher concentration (0.5 mmol, 5 mol %) $\text{Ni}(\text{ClO}_4)_2$ (catalyst). A green nickel complex, isolated from the reaction mixture after 1 h, showed an identical UV-vis spectrum as compared to that of the pure complex, $[\text{Ni}(\text{pap})_3]^{2+}$ (see Experimental Section for details, Supporting Information Figure S26 for spectra). This points to the notion that the ligand L coordinates to Ni(II) salt in the catalytic cycle. Moreover, our attempts to N-arylate two analogous azo-aromatics, viz., azo-benzene (azbz) and azo-bispyridine (azpy), failed under the above experimental conditions. Of the above two azo-aromatic compounds, azbz failed to react with $\text{Ni}^{\text{II}}(\text{ClO}_4)_2$, and no parallel chemical reduction by Zn metal of the reported³⁶ complex, $[\text{Ni}(\text{azpy})_3]^{2+}$, was achieved by us. We also have investigated the reaction of azpy (2 mol) with

Table 5. Products of the Nickel-Catalyzed C–N Coupling Reaction on Azo-Aromatic Compounds with Arylboronic Acids



$\text{Ni}^0(\text{COD})_2$ in an inert atmosphere, which resulted an insoluble material of unknown identity.

Table 4. Nickel-Catalyzed Coupling of Azo-Aromatics with Arylboronic Acid^a

compd	R	Ar	catalyst (mol %)	T (K)	solvent	yield ^d (%)
4a ^{b,c}	H	phenyl (Ph)	1	300	1,4-dioxane	83, ^b 81 ^c
4b ^{b,c}	H	naphthyl	1	300	1,4-dioxane	78, ^b 75 ^c
4c ^{b,c}	H	9-bromoanthracyl	5	323	1,4-dioxane	58, ^b 52 ^c
4d ^{b,c}	H	pyrenyl	5	313	1,4-dioxane	68, ^b 66 ^c
4e ^{b,c}	H	9,9-dimethyl-fluorenyl	2	313	1,4-dioxane	74, ^b 71 ^c
4f ^b	H	3-thiophenyl	1	300	1,4-dioxane	78 ^b
4g ^b	H	<i>p</i> -COCH ₃ -Ph	1	300	1,4-dioxane	62 ^b
4h ^b	H	<i>p</i> -F-Ph	1	313	1,4-dioxane	65 ^b
4i ^b	Cl	H	1	313	1,4-dioxane	68 ^b
4a ^b	H	phenyl (Ph)	1	300	acetonitrile	30 ^b
4a ^b	H	phenyl (Ph)	1	300	THF	66 ^b

^aReaction conditions: L (1 mmol); Ar–B(OH)₂ (1 mmol); catalyst, Ni(II) salt. ^b $\text{Ni}(\text{ClO}_4)_2$. ^c NiCl_2 (0.01 mmol), K_3PO_4 (1 mmol), solvent (5 mL), 300–323 K, 3–6 h. ^dIsolated yield.

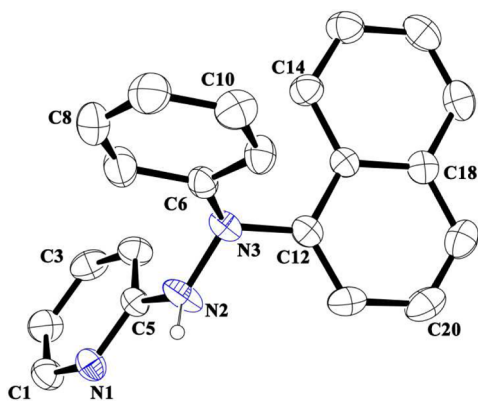


Figure 6. ORTEP view of compound **4b** at 30% probability ellipsoid.

Table 6. Bond Parameters for Compound **4b**

bond param	bond distance (Å)	bond param	bond angle (deg)
N2–N3	1.401(2)	N2–N3–C12	114.36(19)
N2–C5	1.363(3)	C6–N3–C12	119.01(17)
N3–C6	1.436(3)	C6–N3–N2	112.54(17)
N3–C12	1.432(3)	N3–N2–C5	120.26(19)

We wish to add here that aryl boronic acids in the presence of K_3PO_4 are known³⁷ to bring about reduction of Ni(II) complexes to Ni(0) even at room temperature. Moreover, the present Ni^{II}–L complexes are susceptible to facile chemical reduction (vide supra), and each of the above arylation reactions invariably produced the corresponding diaryl compound as a byproduct. Isolated yields of the biaryls were higher in the cases of polycyclic aryl boronic acid. Considering air-sensitivity of Ar^\bullet radical, the above reactions were also tried in an oxygen-free atmosphere, which resulted in higher turnover number (TON) for the reference conversion (Table 7). It may also be worthwhile to note that the above chemical

Table 7. Nickel-Catalyzed Coupling of Azo-Aromatics with Arylboronic Acid in Inert Atmosphere^a

compd	R	Ar	catalyst (mol %)	T (K)	yield ^b (%)
4a	H	phenyl (Ph)	0.5	300	68
4b	H	naphthyl	0.5	300	56
4c	H	9-bromoanthracyl	2	323	38
4d	H	pyrenyl	2	313	42
4e	H	9,9-dimethyl-fluorenyl	1	313	54

^aReaction conditions: L (1 mmol), Ar–B(OH)₂ (1 mmol), Ni(ClO₄)₂ (0.005 mmol), K₃PO₄ (1 mmol), 1,4 dioxane (5 mL), 300–323 K, 3–6 h. ^bIsolated yield.

transformations do not occur in the presence of radical scavengers like TEMPO or BHT. With all this evidence taken together it is concluded that the aforesaid N-arylation reaction is highly specific for the 2-(arylo)pyridine substrates and that the catalytic reactions possibly occur via coordination of L to Ni(II) and coupling of in situ generated radicals.

Properties of Triarylhydrazine. These classes of dyes, in general, are well-known for their use.²² An ideal dye should possess qualities³⁸ of high absorption coefficient, high quantum yield, large Stokes shift, and high chemical and photochemical stability as well. For example, 4,4-difluoro-4-bora-3a,4a-diaza-s-indacene (abbreviated as BODIPY) dye and its derivatives are strongly UV-absorbing small molecules, which are widely used³⁹ to label proteins and DNA. However, most BODIPYs have the disadvantage of small Stokes shifts. In general, synthetic dyes with Stokes shifts >80 nm and also having high fluorescence quantum yields are highly desirable³⁸ to minimize reabsorption of emitted photons.

The compounds, collected in Table 5, have all these desirable properties as dyes: high quantum yields, large Stokes shift (>90 nm), and photostability as well. The photophysical properties of these triarylhydrazines are summarized in Table 8. A comparison of the data indicates that the presence of polycyclic aromatic rings augments the quantum yield of the product considerably. Thus, the quantum yield of >80% was noted in compound **4d**, which contains pyrenyl as one of the aryl groups. The observed Stokes shift of these dyes is unusually high, lying in the range 90–195 nm. To examine the photostability, a solution (10^{−4} M solution in dichloromethane) of a representative sample, **4b**, was irradiated at two wavelengths, 255 and 364 nm, respectively, at room temperature, and its absorption spectra were recorded periodically. The absorption profile was unchanged after 4 h of irradiation. Thus, in addition to thermal and air stability, this dye exhibits significant photostability over a period of time.

CONCLUSION

In this Article, we have introduced a complete description of nickel complexes of azo-aromatic ligands where the ligands are shown to be highly redox-active while the metal ion behaves as a redox innocent center. This situation is just opposite to our common experiences on the redox behavior of most of transition-metal complexes of organic ligands. Our investigation on the possible use of the Ni–L complexes as catalyst finally led to development of an efficient catalytic cycle for N-arylation of 2-(arylo)pyridine using Ni(II) salt as catalyst. Isolated 2-pyridyl-substituted triarylhydrazines are all new and have generated scopes for exploration of their properties as useful dye. Our work on the multiple application possibilities of these dyes is underway and will be reported in due course.

Table 8. Absorbance and Fluorescence Data for New Hydrazine Dyes

compd	absorption, nm (ϵ , M ^{−1} cm ^{−1})	emission (nm)	Stokes shift (nm)	quantum yield (%)	τ_f (ns)
4a	230 (15 160), 245 (13 520), 290 (15 860)	445 (Abs = 290 nm)	155	5.15	2.87
4b	230 (19 800), 245 (10 900), 290 (6000), 335 (2200)	485 (Abs = 290 nm)	195	33.8	5.17
4c	255 (21 000), 380 (1470), 430 (1000)	410 (Abs = 255 nm)	155	40.8	4.47
4d	250 (37 340), 275 (24 440), 300 (16 600), 350 (13 870), 375 (9300)	440 (Abs = 350 nm)	90	85.6	3.89
4e	230 (29 660), 320 (29 482)	415 (Abs = 320 nm)	95	60.0	5.02
4f	230 (27 900), 285 (24 500)	420 (Abs = 285 nm)	135	3.38	5.21

EXPERIMENTAL SECTION

Materials. The salts, $\text{Ni}(\text{COD})_2$, $\text{Ni}(\text{ClO}_4)_2$, and all boronic acids were purchased from Sigma-Aldrich. The salt NiCl_2 was purchased from Spectrochem, India. All other reagents and chemicals were purchased from commercial sources and used without further purifications. Tetrabutylammonium perchlorate was prepared and recrystallized as reported before.²⁷ **Caution!** Perchlorates have to be handled with care and appropriate safety precautions.

Physical Measurements. PerkinElmer Lambda 950 and PerkinElmer LS 55 spectrophotometers were used to record UV–vis and fluorescence spectra, respectively. Infrared spectra were obtained using a PerkinElmer 783 spectrophotometer. ^1H NMR spectra were recorded on a Bruker Avance 300/400/500 MHz spectrometer, and SiMe_4 was used as the internal standard. A PerkinElmer 240C elemental analyzer was used to collect microanalytical data (C, H, N). ESI mass spectra were recorded on a micromass Q-TOF mass spectrometer (serial no. YA 263). All electrochemical measurements were performed using a PC-controlled PAR model 273A electrochemistry system. Cyclic voltammetric experiments were performed under nitrogen atmosphere using a Ag/AgCl reference electrode, with a Pt disk working electrode and a Pt wire auxiliary electrode, in acetonitrile or dichloromethane containing supporting electrolyte, 0.1 M Et_4NClO_4 or 0.1 M Bu_4NClO_4 , respectively. A Pt wire gauge working electrode was used for exhaustive electrolyses. The $E_{1/2}$ for the ferrocenium–ferrocene couple under our experimental condition was 0.39 V. The peak-to-peak separation (ΔE_p) for the Fc/Fc^+ (Fc^+ = ferrocenium ion) couple under this experimental conditions was 80 mV. Room temperature magnetic moment measurements for $[\mathbf{1a}](\text{ClO}_4)_2$ and $\mathbf{2a}$ were carried out with Gouy balance (Sherwood Scientific, Cambridge, U.K.). Emission quantum yields were obtained by using quinine sulfate ($\Phi_F = 0.54$ in 0.1 M H_2SO_4) as reference.

Synthesis. The ligands L^a and L^b were prepared by following the reported procedure.⁴⁰ All other chemicals were of reagent grade and used as received. Solvents were purified and dried prior to use. Preparation and handling of air-sensitive materials were carried out under an inert atmosphere by using standard Schlenk techniques or a glovebox. Complexes $[\mathbf{1}](\text{ClO}_4)_2$ and $\mathbf{2}$ were prepared and characterized as before.²⁵

Synthesis of $\text{Ni}(\text{L}^{a*})_2$, $\mathbf{3a}$. A 133 mg portion of L^a , dissolved in dry dichloromethane, was added dropwise to a freshly prepared dichloromethane solution containing 100 mg of $\text{Ni}(\text{COD})_2$ in a glovebox with constant stirring for 4 h. During this period the color of the solution changes from yellow to brown. The crude mass, obtained by evaporation of solvent in vacuum, was purified by fractional crystallization from dichloromethane and ether solvent mixture. The precipitate was crystallized by slow diffusion of a dichloromethane solution of the compound into hexane. Its yield and characterization data are as follows: yield 90%, ESI-MS, m/z 425 $[\mathbf{3a}]^+$. ^1H NMR (500 MHz, CDCl_3): δ 10.16 (d, 1H, $J = 6$ Hz), 9.03 (d, 2H, $J = 8$ Hz), 7.96 (d, 1H, $J = 8$ Hz), 7.84 (t, 1H, $J = 6$ Hz), 7.72 (t, 1H, $J = 7.0$ Hz), 7.65 (t, 1H, $J = 7.0$ Hz), 7.06 (t, 2H, $J = 7.5$ Hz). ^{13}C NMR (125 MHz, CDCl_3): δ 161.44, 151.37, 134.04, 131.72(2C), 128.09, 124.28, 121.67(2C), 119.77, 117.97. $\lambda_{\text{max/nm}}$ ($\epsilon/\text{M}^{-1}\text{cm}^{-1}$) (dichloromethane): 230 (17 200), 325 (25 500), 415 (6200), 780 (205). Due to its high air sensitivity, reproducible CHN data for complex $\mathbf{3a}$ is not obtained.

An identical compound is also obtained by changing the solvent from dichloromethane to hexane. In this case the compound precipitated out during stirring. The crude solid product was filtered and washed with diethyl ether. The residue was crystallized by slow diffusion of a dichloromethane solution of the compound into hexane. Yield: 85%.

Synthesis of $\text{Ni}(\text{L}^{b*})_2$, $\mathbf{3b}$. This was synthesized similarly as above with an equivalent quantity of L^b in place of L^a . Its yield and characterization data are as follows: yield 86%, ESI-MS, m/z 494 $[\mathbf{3b}]^+$. ^1H NMR (500 MHz, CDCl_3): δ 10.20 (d, 1H, $J = 5$ Hz), 8.96 (d, 2H, $J = 8.5$ Hz), 7.98 (d, 1H, $J = 8$ Hz), 7.90 (t, 1H, $J = 6$ Hz), 7.73 (t, 1H, $J = 7.0$ Hz), 7.00 (d, 1H, $J = 8.5$ Hz). ^{13}C NMR (100 MHz, CDCl_3): δ 161.95, 151.68, 140.18, 134.84, 132.24(2C), 129.04, 122.92(2C), 120.00, 118.59. $\lambda_{\text{max/nm}}$ ($\epsilon/\text{M}^{-1}\text{cm}^{-1}$) (dichloromethane):

225 (17 900), 315 (25 000), 410 (6500), 785 (190). Due to its high air sensitivity, reproducible CHN data for complex $\mathbf{3b}$ is not obtained.

X-ray Crystallography. Crystallographic data for complexes $[\mathbf{1a}]^{2+}$, $\mathbf{2a}$, $\mathbf{3a}$, and $\mathbf{4b}$ are collected in Table 2. Suitable X-ray quality crystals of complexes $[\mathbf{1a}]^{2+}$ and $\mathbf{2a}$ were obtained by the slow evaporation of a dichloromethane–hexane solution of the complex, whereas the crystals of complexes $\mathbf{3a}$ and $\mathbf{4b}$ were obtained by slow diffusion of a dichloromethane solution of the complex into hexane. All data were collected on a Bruker SMART APEX-II diffractometer, equipped with graphite-monochromated $\text{Mo K}\alpha$ radiation ($\lambda = 0.710 73 \text{ \AA}$), and were corrected for Lorentz polarization effects. Data for $\mathbf{1a}(\text{ClO}_4)_2$ follow: A total of 53 081 reflections were collected, of which 12 353 were unique ($R_{\text{int}} = 0.0431$), satisfying the $I > 2\sigma(I)$ criterion, and were used in subsequent analysis. Data for $\mathbf{2a}$ follow: A total of 32 145 reflections were collected, of which 4895 were unique ($R_{\text{int}} = 0.0374$). Data for $\mathbf{3a}$ follow: A total of 50 725 reflections were collected, of which 8393 were unique ($R_{\text{int}} = 0.0357$). Data for $\text{Ni}(\text{L})_2\text{I}_2$ follow: A total of 34 436 reflections were collected, of which 6813 were unique ($R_{\text{int}} = 0.0299$). Data for $\mathbf{4b}$ follow: A total of 18 737 reflections were collected, of which 2846 were unique ($R_{\text{int}} = 0.0520$). During refinement of $\mathbf{3a}$ the observed flack parameter was 0.532 which indicates the possible presence of racemic twin. Thus, the TWIN card has been used before the final refinement which gives a relatively better R factor for the structure. The structures were solved by employing the SHELXS-97 program package^{41a} and were refined by full-matrix least-squares based on F^2 (SHELXL-97).^{41b} All hydrogen atoms were added in calculated positions.

Computational Methods. All DFT calculations presented herein were carried out using the Gaussian 09 program package.⁴² Geometry optimizations were performed without imposing geometric constraints (C_1 symmetry), and stationary points were subsequently confirmed to be minima by vibrational analysis (no imaginary frequencies). All calculations utilized the B3LYP hybrid functional.⁴³ The TZVP basis set⁴⁴ of triple- ζ quality with one set of polarization functions was used on Ni. For all other atoms, C, H, N polarized 6-31G(d,p) basis sets⁴⁵ were used. The broken-symmetry approach first proposed by Ginsberg⁴⁶ and Noodleman⁴⁷ has been employed for all complexes. A range of spin-polarized initial densities was tried in each case (BS(2,2), BS(1,1)), but in all cases different guesses (with the same total multiplicity) converged to the same minimum. Mulliken spin densities were used for analysis of spin populations on ligand and metal centers.⁴⁸

Catalytic Synthesis of Trisubstituted Hydrazines. The catalytic reactions were carried out following a general procedure. A mixture of 2-(aryloxy)pyridine (1.0 equiv), aryl boronic acid (1.0 equiv), $\text{Ni}^{\text{II}}\text{Cl}_2$ (or $\text{Ni}^{\text{II}}(\text{ClO}_4)_2$, 0.01–0.05 equiv), K_3PO_4 (1.0 equiv), and 1,4 dioxane (5 mL) was stirred at 300–325 K in air for 3–5 h. The crude product, thus obtained, was purified in yields on preparative alumina TLC plate using ethyl acetate–hexane (1:10) mixture as eluent. Higher concentration of catalyst and relatively higher temperatures and reaction time were needed for polyaryl aromatic group insertion reactions. The yields and spectral characterization of the products are as follows.

2-(2,2-Diphenylhydrazinyl)pyridine ($\mathbf{4a}$). Pale yellow solid; mp = 154–156 °C. IR (KBr): 3413, 3043, 3005, 2954, 1595, 1490, 1394, 1142, 770 cm^{-1} . ^1H NMR (300 MHz, CDCl_3): δ 6.71 (d, $J = 5$ Hz, 1H), 6.85 (d, $J = 8$ Hz, 1H), 7.02 (d, $J = 3$ Hz, 2H), 7.28 (d, $J = 4$ Hz, 7H), 7.47 (t, $J = 7.5$ Hz, 1H), 7.94 (s, 1H), 8.07 (s, 1H). ^{13}C NMR (75 MHz, CDCl_3): δ 106.3, 115.5, 119.2 (4C), 122.8 (2C), 129.3 (4C), 138.7, 146.4 (2C), 147.8, 159.7. ESI-MS Calcd for $\text{C}_{17}\text{H}_{16}\text{N}_3$ [$\text{M} + \text{H}$]⁺: 262.1328. Found: 262.1338. Anal. Calcd for $\text{C}_{17}\text{H}_{15}\text{N}_3$: C, 78.13; H, 5.79; N, 16.08. Found C, 78.09; H, 5.65; N, 15.87.

2-(2-(Naphthalen-1-yl)-2-phenylhydrazinyl)pyridine ($\mathbf{4b}$). Off white solid; mp = 185–187 °C. IR (KBr): 3400, 3049, 3009, 2953, 1593, 1491, 1392, 1146, 1280, 771 cm^{-1} . ^1H NMR (500 MHz, CDCl_3): δ 6.70 (t, $J = 6$ Hz, 1H), 6.85–6.91 (m, 3H), 7.08 (d, $J = 8$ Hz, 1H), 7.18 (t, $J = 8$ Hz, 2H), 7.42–7.53 (m, 3H), 7.59 (d, $J = 7$ Hz, 1H), 7.65 (s, 1H), 7.78 (d, $J = 8.5$ Hz, 1H), 7.89–7.94 (m, 2H), 8.05 (d, $J = 5$ Hz, 1H). ^{13}C NMR (125 MHz, CDCl_3): δ 106.8, 115.4 (2C), 115.6, 120.9, 122.9, 123.8, 126.3 (2C), 126.6, 127.3, 128.8, 129.2 (2C),

129.7, 135.0, 138.7, 142.8, 147.8, 149.6, 159.9. ESI-MS Calcd for $C_{21}H_{18}N_3$ $[M + H]^+$: 312.1484. Found: 312.1596. Anal. Calcd for $C_{21}H_{17}N_3$: C, 81.00; H, 5.50; N 13.49. Found C, 80.53; H, 5.46; N, 13.46.

2-(2-(10-Bromoanthracen-9-yl)-2-phenylhydrazinyl)pyridine (4c). Pale green solid; mp = 172–174 °C. IR (KBr): 3408, 3042, 3019, 2943, 1591, 1497, 1382, 1270, 1143, 774 cm^{-1} . 1H NMR (500 MHz, $CDCl_3$): δ 6.47 (t, J = 8.5 Hz, 1H), 7.46–7.53 (m, 3H), 7.60 (t, J = 9 Hz, 2H), 7.80–7.87 (m, 4H), 8.00 (d, J = 8.5 Hz, 1H), 8.25–8.27 (m, 2H), 8.31–8.33 (m, 2H), 8.45 (t, J = 8.5 Hz, 1H), 8.52 (d, J = 9 Hz, 1H). ^{13}C NMR (75 MHz, $CDCl_3$): δ 118.61, 122.80, 123.75 (2C), 125.43 (2C), 126.10 (2C), 127.15 (2C), 128.43 (2C), 128.92 (2C), 129.32 (2C), 130.21, 132.35, 132.58, 134.28, 137.98 (2C), 138.56, 152.49, 162.95. ESI-MS Calcd for $C_{25}H_{19}N_3Br$ $[M + H]^+$: 440.0684. Found: 440.0884. Anal. Calcd for $C_{25}H_{18}N_3Br$: C, 68.19; H, 4.12; N, 9.54. Found C, 68.17; H, 4.11, N, 9.52.

2-(2-Phenyl-2-(pyren-1-yl)hydrazinyl)pyridine (4d). Yellowish solid; mp = 164–166 °C. IR (KBr): 3402, 3043, 3015, 2941, 1597, 1491, 1385, 1278, 1148, 772 cm^{-1} . 1H NMR (500 MHz, $CDCl_3$): δ 6.63 (t, J = 7 Hz, 1H), 6.80–6.84 (m, 3H), 7.06–7.12 (m, 3H), 7.40 (d, J = 7.5 Hz, 1H), 7.92–8.08 (m, 4H), 8.09–8.16 (m, 4H), 8.31 (d, J = 8 Hz, 1H). ^{13}C NMR (125 MHz, $CDCl_3$): δ 163.08, 152.60, 138.50, 137.69, 132.57, 132.32, 131.48, 131.19(2C), 129.90, 129.34, 129.04, 127.68, 127.43, 127.30, 126.71, 126.37, 126.12, 125.53, 125.37, 125.30, 125.11, 123.79, 123.56(2C), 122.82, 118.61. ESI-MS Calcd for $C_{27}H_{19}N_3Na$ $[M + Na]^+$: 408.1477. Found: 408.5035. Anal. Calcd for $C_{27}H_{19}N_3$: C, 84.13; H, 4.97, N, 10.90. Found C, 83.64; H, 4.90; N, 10.81.

2-(2-(9,9-Dimethyl-fluoren-2-yl)-2-phenylhydrazinyl)pyridine (4e). Off white solid; mp = 187–189 °C. IR (KBr): 3404, 3042, 3006, 2952, 1583, 1498, 1396, 1287, 1151, 773 cm^{-1} . 1H NMR (500 MHz, $CDCl_3$): δ 1.29 (s, 6H), 6.53 (t, J = 6 Hz, 1H), 6.75 (d, J = 8.5 Hz, 1H), 6.88 (t, J = 7 Hz, 1H), 7.11–7.19 (m, 7H), 7.26 (d, J = 7 Hz, 2H), 7.32 (d, J = 8.5 Hz, 1H), 7.46–7.51 (m, 2H), 7.91 (d, J = 5 Hz, 1H), 8.22 (s, 1H). ^{13}C NMR (125 MHz, $CDCl_3$): δ 27.2 (2C), 46.9, 106.3, 114.0, 115.4, 118.7, 118.8 (2C), 119.5, 120.6, 122.5, 122.6, 126.6, 127.0, 129.3 (2C), 134.4, 138.5, 139.0, 145.9, 146.8, 147.9, 153.5, 155.1, 159.9. ESI-MS Calcd for $C_{26}H_{24}N_3$ $[M + H]^+$: 378.1892. Found: 378.1894. Anal. Calcd for $C_{26}H_{23}N_3$: C, 82.73; H, 6.14, N, 11.13. Found C, 81.63; H, 5.82; N, 10.81.

2-Phenyl-1-(pyridin-2-yl)-2-(thiophen-3-yl)hydrazine (4f). Off white solid; mp = 143–145 °C. IR (KBr): 3414, 3048, 3016, 2957, 1582, 1497, 1393, 1285, 1147, 778 cm^{-1} . 1H NMR (500 MHz, $CDCl_3$): δ 6.63–6.66 (m, 1H), 6.75–6.77 (m, 2H), 6.88–6.95 (m, 2H), 7.13–7.20 (m, 5H), 7.39–7.42 (m, 1H), 8.04 (d, J = 5 Hz, 1H). ^{13}C NMR (125 MHz, $CDCl_3$): δ 106.5, 109.4, 115.8, 117.2 (2C), 122.2, 122.4, 125.6, 129.3 (2C), 138.6, 145.8, 147.3, 148.0, 159.5. ESI-MS Calcd for $C_{15}H_{14}N_3S$ $[M + H]^+$: 268.0830. Found: 268.1231. Anal. Calcd for $C_{15}H_{14}N_3S$: C, 67.39; H, 4.90, N, 15.72. Found: C, 67.11; H, 4.82; N, 15.61.

1-(4-(1-Phenyl-2-(pyridin-2-yl)hydrazinyl)phenyl)ethanone (4g). Off white solid; mp = 157–159 °C. IR (KBr): 3413, 3044, 3018, 2951, 1732, 1572, 1493, 1383, 1282, 1146, 771 cm^{-1} . 1H NMR (500 MHz, $CDCl_3$): δ 2.52 (s, 3H), 6.74 (s, 2H), 7.14–7.19 (m, 3H), 7.33–7.38 (m, 4H), 7.48 (t, J = 8 Hz, 1H), 7.84 (d, J = 8 Hz, 2H), 8.10 (s, 1H). ^{13}C NMR (125 MHz, $CDCl_3$): δ 26.3, 106.3, 115.4 (2C), 116.1, 122.4 (2C), 125.3, 129.7 (2C), 130.3, 130.4 (2C), 138.7, 144.5, 148.0, 150.9, 159.0, 196.5. ESI-MS Calcd for $C_{19}H_{18}N_3O$ $[M + H]^+$: 304.1372. Found: 304.1403. Anal. Calcd for $C_{19}H_{18}N_3O$: C, 75.23; H, 5.65, N, 13.85. Found: C, 75.11; H, 4.90; N, 13.61.

2-(4-Fluorophenyl)-2-phenyl-1-(pyridin-2-yl)hydrazine (4h). Off white solid; mp = 151–153 °C. IR (KBr): 3423, 3054, 3028, 2957, 1579, 1492, 1388, 1286, 1143, 775 cm^{-1} . 1H NMR (500 MHz, $CDCl_3$): δ 6.78–6.81 (m, 1H), 6.90–6.96 (m, 4H), 7.18–7.24 (m, 5H), 7.43–7.51 (m, 2H), 8.22 (s, 1H). ESI-MS Calcd for $C_{17}H_{15}N_3F$ $[M + H]^+$: 280.1250. Found: 280.1248. Anal. Calcd for $C_{17}H_{14}N_3F$: C, 73.10; H, 5.05, N, 15.04. Found: C, 72.56; H, 4.90; N, 14.68.

2-(2-(4-Chlorophenyl)-2-phenylhydrazinyl)pyridine (4i). Off white solid; mp = 159–161 °C. IR (KBr): 3418, 3034, 3008, 2954, 1576, 1498, 1393, 1292, 1145, 773 cm^{-1} . 1H NMR (500 MHz, $CDCl_3$): δ

6.86–6.89 (m, 2H), 7.17–7.20 (m, 2H), 7.33 (d, J = 7 Hz, 1H), 7.41 (t, J = 8 Hz, 2H), 7.46–7.53 (m, 2H), 7.61 (d, J = 8 Hz, 2H), 7.88 (d, J = 8 Hz, 1H), 7.98 (d, J = 8 Hz, 1H). ^{13}C NMR (125 MHz, $CDCl_3$): δ 116.9, 118.3 (2C), 121.9 (2C), 123.8, 126.1, 126.3, 128.1, 128.7 (2C), 129.4 (2C), 134.9, 138.4, 143.8, 160.4. ESI-MS Calcd for $C_{17}H_{15}ClN_3$ $[M + H]^+$: 296.0955. Found: 296.3767. Anal. Calcd for $C_{17}H_{15}ClN_3$: C, 69.03; H, 4.77, N, 11.99. Found C, 70.11; H, 4.90; N, 12.04.

Isolation of $[1a]^{2+}$ During the Course of the Reaction. A mixture of 2-(aryloxy)pyridine (1.0 equiv), naphthyl boronic acid (1.0 equiv), $Ni^{II}(ClO_4)_2$ (0.05 equiv), K_3PO_4 (1.0 equiv), and 1,4-dioxane (5 mL) was stirred at 300 K in air for 1 h. The solvent was evaporated in a rotary evaporator. The crude mixture thus obtained was subsequently washed with water and ethyl acetate to remove unreacted aryl boronic acid, 2-(aryloxy)pyridine (L), base (K_3PO_4), and triarylhydrazine (4b) as well. A tiny quantity of green residue was isolated and characterized as $[1a]^{2+}$ by its UV–vis spectrum.

■ ASSOCIATED CONTENT

Supporting Information

Figures, tables, scheme, and CIF files giving crystallographic details and selected bond parameters of the complexes $Ni(L^a)_2I_2$ and two isomers of **3a**, ORTEP of two isomers of **3a** and $Ni(L^a)_2I_2$, cyclic voltammograms at different scan rates of $[1a]^{2+}$ and **2a**, ORTEP representation of $Ni(L^a)_2I_2$, NMR spectra of **3a**, **b** and **4a–i**, ESI-MS spectra of **3a** and **4a–i**, UV–vis spectra of the complexes $[1a]^{2+}$, **2a**, **3a**, and **4a–f**, fluorescence spectra of **4a–f**, and Cartesian coordinates of the optimized structure **3a**. This material is available free of charge via the Internet at <http://pubs.acs.org>.

■ AUTHOR INFORMATION

Corresponding Author

*E-mail: icsg@iacs.res.in.

Present Address

[§]Department of Chemistry, Indian Institutes of Engineering Science and Technology, Shibpur, Howrah-711 103, India.

Notes

The authors declare no competing financial interest.

■ ACKNOWLEDGMENTS

The research was supported by Council for Scientific and Industrial Research (CSIR) and Department of Science and Technology (DST), India, funded projects 01(2714)/13/EMR-II and SR/S1/IC/0031/2010, respectively. S.G. sincerely thanks DST for a J. C. Bose fellowship. Crystallography was performed at the DST funded National Single Crystal Diffractometer Facility at the Department of Inorganic Chemistry, IACS. D.S., P.G., T.C., and H.D. are thankful to the Council of Scientific and Industrial Research for their fellowship support.

■ REFERENCES

- (1) Jørgensen, C. K. *Coord. Chem. Rev.* **1966**, *1*, 164–178.
- (2) Chirik, P. J.; Wieghardt, K. *Science* **2010**, *327*, 794–795.
- (3) (a) Shivakumar, M.; Pramanik, K.; Ghosh, P.; Chakravorty, A. *Inorg. Chem.* **1998**, *37*, 5968–5969. (b) Pramanik, K.; Shivakumar, M.; Ghosh, P.; Chakravorty, A. *Inorg. Chem.* **2000**, *39*, 195–199. (c) Kaim, W. *Inorg. Chem.* **2011**, *50*, 9752–9765. (d) Sarkar, B.; Patra, S.; Fiedler, J.; Sunoj, R. B.; Janardana, D.; Mobin, S. M.; Niemeyer, M.; Lahiri, G. K.; Kaim, W. *Angew. Chem., Int. Ed.* **2005**, *44*, S655–S658. (e) Sarkar, B.; Patra, S.; Fiedler, J.; Sunoj, R. B.; Janardana, D.; Lahiri, G. K.; Kaim, W. *J. Am. Chem. Soc.* **2008**, *130*, 3532–3542. (f) Kaim, W. *Coord. Chem. Rev.* **2001**, *219–221*, 463–488.

- (4) (a) Goswami, S.; Sengupta, D.; Paul, N. D.; Mondal, T. K.; Goswami, S. *Chem.—Eur. J.* **2014**, *20*, 6103–6111. (b) Paul, N. D.; Rana, U.; Goswami, S.; Mondal, T. K.; Goswami, S. *J. Am. Chem. Soc.* **2012**, *134*, 6520–6523. (c) Ghosh, P.; Samanta, S.; Roy, S. K.; Demeshko, S.; Meyer, F.; Goswami, S. *Inorg. Chem.* **2014**, *53*, 4678–4686. (d) Samanta, S.; Ghosh, P.; Goswami, S. *Dalton Trans.* **2012**, *41*, 2213–2226. (e) Ghosh, P.; Samanta, S.; Roy, S. K.; Joy, S.; Krämer, T.; McGrady, J. E.; Goswami, S. *Inorg. Chem.* **2013**, *52*, 14040–14049. (f) Joy, S.; Krämer, T.; Paul, N. D.; Banerjee, P.; McGrady, J. E.; Goswami, S. *Inorg. Chem.* **2011**, *50*, 9993–10004. (g) Paul, N.; Samanta, S.; Goswami, S. *Inorg. Chem.* **2010**, *49*, 2649–2655. (h) Sanyal, A.; Chatterjee, S.; Castiñeiras, A.; Sarkar, B.; Singh, P.; Fiedler, J.; Zális, S.; Kaim, W.; Goswami, S. *Inorg. Chem.* **2007**, *46*, 8584–8593. (i) Sanyal, A.; Banerjee, P.; Lee, G.-H.; Peng, S.-M.; Hung, C.-H.; Goswami, S. *Inorg. Chem.* **2004**, *43*, 7456–7462. (j) Samanta, S.; Singh, P.; Fiedler, J.; Zális, S.; Kaim, W.; Goswami, S. *Inorg. Chem.* **2008**, *47*, 1625–1633.
- (5) Das, A.; Scherer, T. M.; Mobin, S. M.; Kaim, W.; Lahiri, G. K. *Chem.—Eur. J.* **2012**, *18*, 11007–11018.
- (6) (a) Lever, A. B. P. *Coord. Chem. Rev.* **2010**, *254*, 1397–1405. (b) Lever, A. B. P.; Masui, H.; Metcalfe, R. A.; Stufkens, D. J.; Dodsworth, E. S.; Auburn, P. R. *Coord. Chem. Rev.* **1993**, *125*, 317–332. (c) Gorelsky, S. I.; Dodsworth, E. S.; Lever, A. B. P.; Vlcek, A. A. *Coord. Chem. Rev.* **1998**, *174*, 469–494.
- (7) (a) Pierpont, C. G. *Inorg. Chem.* **2011**, *50*, 9766–9772. (b) Gray, H. B. *Coord. Chem. Rev.* **1966**, *1*, 156–163. (c) Dithiolene Chemistry: Synthesis, Properties, and Applications. In *Progress in Inorganic Chemistry*; Stiefel, E. I., Ed.; John Wiley and Sons: Hoboken, NJ, 2004; Vol. 52. (d) Forum Issue on Redox Noninnocent Ligands: *Inorg. Chem.* **2011**, *50*, 9737–9740.
- (8) (a) Lu, C. C.; Weyhermüller, T.; Bill, E.; Wieghardt, K. *Inorg. Chem.* **2009**, *48*, 6055–6064. (b) Lu, C. C.; Bill, E.; Weyhermüller, T.; Bothe, E.; Wieghardt, K. *J. Am. Chem. Soc.* **2008**, *130*, 3181–3197. (c) Bart, S. C.; Chłopek, K.; Bill, E.; Bouwkamp, M. W.; Lobkovsky, E.; Neese, F.; Wieghardt, K.; Chirik, P. J. *J. Am. Chem. Soc.* **2006**, *128*, 13901–13912. (d) Wang, M.; Weyhermüller, T.; England, J.; Wieghardt, K. *Inorg. Chem.* **2013**, *52*, 12763–12776. (e) Scarborough, C. C.; Lancaster, K. M.; DeBeer, S.; Weyhermüller, T.; Sproules, S.; Wieghardt, K. *Inorg. Chem.* **2012**, *51*, 3718–3732. (f) Wang, M.; England, J.; Weyhermüller, T.; Kokatam, S.-L.; Pollock, C. J.; DeBeer, S.; Shen, J.; Yap, G. P. A.; Theopold, K. H.; Wieghardt, K. *Inorg. Chem.* **2013**, *52*, 4472–4487. (g) Wile, B. M.; Trovitch, R. J.; Bart, S. C.; Tondreau, A. M.; Lobkovsky, E.; Milsman, C.; Bill, E.; Wieghardt, K.; Chirik, P. J. *Inorg. Chem.* **2009**, *48*, 4190–4200. (h) Chaudhuri, P.; Verani, C. N.; Bill, E.; Bothe, E.; Weyhermüller, T.; Wieghardt, K. *J. Am. Chem. Soc.* **2001**, *123*, 2213.
- (9) (a) Chaudhuri, P.; Hess, M.; Flörke, U.; Wieghardt, K. *Angew. Chem., Int. Ed.* **1998**, *37*, 2217–2220. (b) Chaudhuri, P.; Hess, M.; Müller, J.; Hildenbrand, K.; Bill, E.; Weyhermüller, T.; Wieghardt, K. *J. Am. Chem. Soc.* **1999**, *121*, 9599–9610. (c) Mukherjee, C.; Pieper, U.; Bothe, E.; Bachler, V.; Bill, E.; Weyhermüller, T.; Chaudhuri, P. *Inorg. Chem.* **2008**, *47*, 8943–8956.
- (10) (a) Lyaskovskyy, V.; de Bruin, B. *ACS Catal.* **2012**, *2*, 270–279. (b) Dzik, W. I.; Vlucht, J. I. V. D.; Reek, J. N. H.; Bruin, B. D. *Angew. Chem., Int. Ed.* **2011**, *50*, 3356–3358. (c) Smith, A. L.; Hardcastle, K. I.; Soper, J. D. *J. Am. Chem. Soc.* **2010**, *132*, 14358–14360. (d) Praneeth, V. K. K.; Ringenber, M. R.; Ward, T. R. *Angew. Chem., Int. Ed.* **2012**, *51*, 10228–10234.
- (11) (a) Kaim, W. *Dalton Trans.* **2003**, 761–768. (b) Kaim, W.; Schwederski, B. *Coord. Chem. Rev.* **2010**, *254*, 1580–1588.
- (12) (a) Vlucht, J. I. V. D.; Reek, J. N. H. *Angew. Chem., Int. Ed.* **2009**, *48*, 8832–8846. (b) Grützmacher, H. *Angew. Chem., Int. Ed.* **2008**, *47*, 1814–1818.
- (13) Luca, O. R.; Crabtree, R. H. *Chem. Soc. Rev.* **2013**, *42*, 1440–1459.
- (14) (a) Schmidt, E. W. *Hydrazine and its Derivatives: Preparation, Properties, Applications*, 2nd ed.; Wiley-Interscience: Hoboken, NJ, 2001. (b) Syngenta Limited. Process for the Preparation of Aryl Hydrazone and Aryl Hydrazine. PCT Patent Application WO 03/035604 A1, 2001.
- (15) (a) Ragnarsson, U. *Chem. Soc. Rev.* **2001**, *30*, 205–213. (b) Zhang, R.; Durkin, J. P.; Windsor, W. T. *Bioorg. Med. Chem. Lett.* **2002**, *12*, 1005–1008. (c) Lee, T.-W.; Cherney, M. M.; Huitema, C.; Liu, J.; James, K. E.; Powers, J. C.; Eltis, L. D.; James, M. N. G. *J. Mol. Biol.* **2005**, *354*, 1137–1151.
- (16) Abrams, M. J.; Juweid, M.; TenKate, C. I.; Schwartz, D. A.; Hauser, M. M.; Gaul, F. E.; Fucello, A. J.; Rubin, R. H.; Strauss, H. W.; Fischman, A. J. *J. Nucl. Med.* **1990**, *31*, 2022–2028.
- (17) Rose, D. J.; Maresca, K. P.; Nicholson, T.; Davison, A.; Jones, A. G.; Babich, J.; Fischman, A.; Graham, W.; DeBord, J. R. D.; Zubietta, J. *Inorg. Chem.* **1998**, *37*, 2701–2716.
- (18) Edwards, D. S.; Liu, S.; Harris, A. R.; Poirier, M. J.; Ewels, B. A. *Bioconjugate Chem.* **1999**, *10*, 803–807.
- (19) Harris, T. D.; Sworin, M.; Williams, N.; Rajopadhye, M.; Dampousse, P. R.; Glowacka, D.; Poirier, M. J.; Yu, K. *Bioconjugate Chem.* **1999**, *10*, 808–814.
- (20) Alberto, R.; Schibli, R.; Schubiger, A. P.; Abram, U.; Pietzsch, H.-J.; Johannsen, B. *J. Am. Chem. Soc.* **1999**, *121*, 6076–6077.
- (21) (a) Buchwald, S. L.; Wagaw, S.; Geis, O. Metal-Catalyzed Arylations of Hydrazines, Hydrazones, and Related Substrates. U.S. Patent US 006235936 B1, 2001. (b) Wagaw, S.; Yang, B. H.; Buchwald, S. L. *J. Am. Chem. Soc.* **1998**, *120*, 6621–6622.
- (22) (a) Muniz, K.; Iglesias, A. *Angew. Chem., Int. Ed.* **2007**, *46*, 6350–6353. (b) Lundgren, R. J.; Stradiotto, M. *Angew. Chem., Int. Ed.* **2010**, *49*, 8686–8690.
- (23) Gu, L.; Neo, B. S.; Zhang, Y. *Org. Lett.* **2011**, *13*, 1872–1874.
- (24) Arterburn, J. B.; Rao, K. V.; Ramdas, R.; Dible, B. R. *Org. Lett.* **2001**, *3*, 1351–1354.
- (25) Raghavendra, B. S.; Chakravorty, A. *Indian J. Chem.* **1976**, *14A*, 166–169.
- (26) Buriez, O.; Moretto, L. M.; Ugo, P. *Electrochim. Acta* **2006**, *52*, 958–964.
- (27) Goswami, S.; Mukherjee, R. N.; Chakravorty, A. *Inorg. Chem.* **1983**, *22*, 2825–2832.
- (28) Blanchard, S.; Neese, F.; Bothe, E.; Bill, E.; Weyhermüller, T.; Wieghardt, K. *Inorg. Chem.* **2005**, *44*, 3636–3656.
- (29) Dougan, S. J.; Melchart, M.; Habtemariam, A.; Parsons, S.; Sadler, P. J. *Inorg. Chem.* **2006**, *45*, 10882–10894.
- (30) (a) Lu, C. C.; Bill, E.; Weyhermüller, T.; Bothe, E.; Wieghardt, K. *Inorg. Chem.* **2007**, *46*, 7880–7889. (b) Lu, C. C.; Bill, E.; Weyhermüller, T.; Bothe, E.; Wieghardt, K. *J. Am. Chem. Soc.* **2008**, *130*, 3181–3197.
- (31) (a) Nicolaou, K. C.; Bulger, P. G.; Sarlah, D. *Angew. Chem., Int. Ed.* **2005**, *44*, 4442–4489. (b) Meijere, A. d.; Diederich, F. *Metal-Catalyzed Cross-Coupling Reactions*; Wiley-VCH: Weinheim, 2014.
- (32) (a) Hartwig, J. F. *Synlett* **2006**, 1283–1294. (b) Buchwald, S. L.; Mauger, C.; Mignani, G.; Scholz, U. *Adv. Synth. Catal.* **2006**, *348*, 23–39. (c) Wolfe, J. P.; Wagaw, S.; Marcoux, J. F.; Buchwald, S. L. *Acc. Chem. Res.* **1998**, *31*, 805–818.
- (33) (a) Ma, Q. U.S. Patent US 7608568 B2, 2009. (b) Koenig, K.-H. U.S. Patent US 3683026, 1972.
- (34) Gulaczyk, I.; Krezglewski, M.; Valentin, A. *J. Mol. Spectrosc.* **2003**, *220*, 132–136.
- (35) Wu, R.; Brutschy, B. *J. Phys. Chem. A* **2004**, *108*, 9715–9720.
- (36) Baldwin, D. A.; Lever, A. B. P.; Parish, R. V. *Inorg. Chem.* **1969**, *8*, 107–115.
- (37) Ge, S.; Hartwig, J. F. *Angew. Chem., Int. Ed.* **2012**, *51*, 12837–12841.
- (38) Araneda, J. F.; Piers, W. E.; Heyne, B.; Parvez, M.; McDonald, R. *Angew. Chem., Int. Ed.* **2011**, *50*, 12214–12217.
- (39) Boens, N.; Leen, V.; Dehaen, W. *Chem. Soc. Rev.* **2012**, *41*, 1130–1172.
- (40) (a) Campbell, N.; Henderson, A. W.; Taylor, D. *J. Chem. Soc.* **1953**, 1281–1285. (b) Prievisch, B.; Rück-Braun, K. *J. Org. Chem.* **2005**, *70*, 2350–2352.

- (41) (a) Sheldrick, G. M. *Acta Crystallogr., Sect. A* **1990**, *46*, 467–473. (b) Sheldrick, G. M. *SHELXL 97, Program for the Refinement of Crystal Structures*; University of Göttingen: Göttingen, Germany, 1997.
- (42) Frisch, M. J.; Trucks, G. W.; Schlegel, H. B.; Scuseria, G. E.; Robb, M. A.; Cheeseman, J. R.; Montgomery, J. A., Jr.; Vreven, T.; Kudin, K. N.; Burant, J. C.; Millam, J. M.; Iyengar, S. S.; Tomasi, J.; Barone, V.; Mennucci, B.; Cossi, M.; Scalmani, G.; Rega, N.; Petersson, G. A.; Nakatsuji, H.; Hada, M.; Ehara, M.; Toyota, K.; Fukuda, R.; Hasegawa, J.; Ishida, M.; Nakajima, T.; Honda, Y.; Kitao, O.; Nakai, H.; Klene, M.; Li, X.; Knox, J. E.; Hratchian, H. P.; Cross, J. B.; Bakken, V.; Adamo, C.; Jaramillo, J.; Gomperts, R.; Stratmann, R. E.; Yazyev, O.; Austin, A. J.; Cammi, R.; Pomelli, C.; Ochterski, J. W.; Ayala, P. Y.; Morokuma, K.; Voth, G. A.; Salvador, P.; Dannenberg, J. J.; Zakrzewski, V. G.; Dapprich, S.; Daniels, A. D.; Strain, M. C.; Farkas, O.; Malick, D. K.; Rabuck, A. D.; Raghavachari, K.; Foresman, J. B.; Ortiz, J. V.; Cui, Q.; Baboul, A. G.; Clifford, S.; Cioslowski, J.; Stefanov, B. B.; Liu, G.; Liashenko, A.; Piskorz, P.; Komaromi, I.; Martin, R. L.; Fox, D. J.; Keith, T.; Al-Laham, M. A.; Peng, C. Y.; Nanayakkara, A.; Challacombe, M.; Gill, P. M. W.; Johnson, B.; Chen, W.; Wong, M. W.; Gonzalez, C.; Pople, J. A. *Gaussian 09, Revision A.02*; Gaussian, Inc.: Wallingford, CT, 2010.
- (43) (a) Becke, A. D. *J. Chem. Phys.* **1993**, *98*, 5648–5652. (b) Lee, C.; Yang, W.; Parr, R. G. *Phys. Rev. B: Condens. Matter Mater. Phys.* **1988**, *37*, 785–789. (c) Vosko, S. H.; Wilk, L.; Nusair, M. *Can. J. Phys.* **1980**, *58*, 1200–1211. (d) Stephens, P. J.; Devlin, F. J.; Chabalowski, C. F.; Frisch, M. J. *J. Phys. Chem.* **1994**, *98*, 11623–11627.
- (44) Schäfer, A.; Huber, C.; Ahlrichs, R. *J. Chem. Phys.* **1994**, *100*, 5829–5835.
- (45) Schäfer, A.; Horn, H.; Ahlrichs, R. *J. Chem. Phys.* **1992**, *97*, 2571–2577.
- (46) Ginsberg, A. P. *J. Am. Chem. Soc.* **1980**, *102*, 111–117.
- (47) (a) Noodleman, L.; Case, D. A.; Aizman, A. *J. Am. Chem. Soc.* **1988**, *110*, 1001–1005. (b) Noodleman, L.; Davidson, E. R. *Chem. Phys.* **1986**, *109*, 131–143. (c) Noodleman, L.; Norman, J. G., Jr.; Osborne, J. H.; Aizman, C.; Case, D. A. *J. Am. Chem. Soc.* **1985**, *107*, 3418–3426. (d) Noodleman, L. *J. Chem. Phys.* **1981**, *74*, 5737–5743.
- (48) Mulliken, R. S. *J. Chem. Phys.* **1955**, *23*, 1833–1840.